Low-Frequency Anomalies in the NMC MRF Model and Reality

WILBUR Y. CHEN AND HUUG VAN DEN DOOL

Climate Prediction Center, NOAA/NWS/NCEP, Washington, D.C.

(Manuscript received 24 August 1993, in final form 26 October 1994)

ABSTRACT

A low-resolution version of the National Meteorological Center's global spectral model was used to generate a 10-year set of simulated daily meteorological data. Wintertime low-frequency large-amplitude anomalies were examined and compared with those observed in the real atmosphere. The geographical distributions of the mean and variance of model and real atmosphere show some resemblance. However, careful comparisons reveal distinct regions where short-term climate anomalies prefer to develop. The model's low-frequency anomalies (LFAs) over the North Pacific (North Atlantic) tend to occur about 1500 miles east (southeast) of those observed, locating themselves much closer to the western continents. Because of the misplacement of the model's LFA centers, their associated circulation patterns deviate substantially from those observed.

The frequency distributions of the LFAs for both the model and reality display large skewness. The positive and negative large LFAs were, therefore, examined separately, and four-way intercomparisons were conducted between the model, the observed, the positive, and the negative LFAs. The separate analyses resulted in distinguishable circulation patterns between the positive and negative large LFAs, which cannot possibly be identified if a linear analysis tool, such as an empirical orthogonal function analysis, were used to extract the most dominant mode of the circulations. Despite pronounced misplacement of large LFAs of both polarities and a general underestimation of their magnitudes, the model does have the capability of persisting its short-term climate anomaly at certain geographical locations. Over the North Pacific, the model's positive LFAs persist as long or longer than those found in reality, while its negative LFAs persist only one-fourth as long (10 versus 40 days).

The principal storm tracks and mean zonal wind at 250 mb (U250) were also examined to supplement the low-frequency anomaly investigation. Contrasting with observations, the model's U250s display considerable eastward extension and its storm tracks near the jet exit show substantial equatorward displacement over both the North Pacific and the North Atlantic oceans. These model characteristics are consistent with the behavior that the model's large LFAs also prefer to develop over the regions far east and southeast of those observed in the real atmosphere.

1. Introduction

Atmospheric circulation fluctuates with a wide range of space and timescales. A low-frequency large-amplitude anomaly can result in catastrophic drought, pronounced heat wave, devastating deep freeze, or other severe weather phenomena. Interest in the nature and sources of low-frequency variabilities has therefore been very strong. Furthermore, the low-frequency variations are thought to be more predictable and this gives rise to hope for the extended range forecasts of these phenomena. In addition to observational and simple model studies, applications of general circulation models (GCM) in order to gain further insights into processes leading to short-term climate anomalies is receiving increasing attention.

This study will attempt to determine whether a GCM can create and maintain short-term climate anomalies, especially long-lasting blocking episodes. In a recent investigation on the prediction of blocking flows, Tibaldi and Molteni (1990) found a severe underestimation of blocking frequency in the European Centre for Medium-Range Weather Forecasts (ECMWF) medium range forecasts. The recent dynamical extended range forecasting (DERF) experiments conducted at the National Meteorological Center (NMC) (Tracton et al. 1989) also indicate that a large portion of the unskillful forecasts can be traced to the model's inability to predict the evolution of blocking events beyond a few days into the forecast.

We are curious whether the underestimation of blocking episodes is due to the deficiency of the model's dynamics or simply the model's inability to place the prominent weather anomalies at the right location. We seek to determine whether a comprehensive GCM is capable of generating short-term climate anomalies, persistent troughs in addition to blocking ridges, and maintain them as long as those observed. Employing the medium-range forecast (MRF) model developed at NMC (Sela 1980; Kanamitsu 1989), we will attempt to document the low-frequency and large amplitude

Corresponding author address: Dr. Wilbur Y. Chen, Climate Analysis Center, NOAA/National Meteorological Center, Washington, DC 20233.
E-mail: wd51wc@sunl.wwb.noaa.gov

variability of this model and compare it with the real atmosphere. A 10-year integration was generated by Van den Dool et al. (1991). Using this dataset, Anderson (1993) has documented the climatology of blocking in this GCM. By emphasizing the characteristics of low-frequency and large-amplitude variability, this investigation compliments Anderson's and together brings forth a more complete picture of the capability as well as the deficiency of the model for short-term climate prediction.

Based on NMC's operationally analyzed data for the last few decades, a fairly comprehensive understanding about the atmospheric general circulation has already been gained (e.g., Blackmon 1976; Blackmon et al. 1977; Wallace and Blackmon 1983; Dole and Gordon 1983). During wintertime, for instance, the major height fluctuation centers were found over the North Pacific and Atlantic Oceans and the Siberian arctic. The high-frequency principal storm tracks were found as elongated maxima of variability over the oceans slightly north of the jetstream latitudes, whereas the maxima of low-frequency variability were located in the central and eastern oceans near the exits of the principal storm tracks (Wallace and Blackmon 1983; Dole and Gordon 1983).

The skewness and kurtosis (the third and fourth moments) of the atmospheric fluctuations have been investigated by White (1980). The dynamical implication of skewness has gained increased attention in the recent years. Using a simple nonlinear model, Vautard et al. (1988) found a link between the statistical asymmetries and the positions of the storm tracks. Knox and Hay (1985) suggested that the positive skewness on the northern flank of the storm tracks is a reflection of blocking activities. Exploring the relationship between the baroclinic wave activities and the life cycles of the low-frequency circulation anomalies, Nakamura and Wallace (1990, 1991) found that the skewness pattern shifts northward and southward with the storm track and the meridional gradient of the skewness increases with the intensity of the baroclinic wave activities.

Due to the dynamical significance of the skewed distribution of the low-frequency anomalies, we would like to investigate whether positive or negative anomalies contribute more to the variance maxima mentioned above. Do all variance maxima have the same composition? They may consist of different frequency distributions suggesting different physical processes leading to their respective composition. Returning to the model's characteristics, how faithfully does a comprehensive GCM generate short-term climate anomalies? Where do they prefer to develop and how persistent are they?

The NMC MRF model was employed to generate 10 years of daily simulated meteorological data (Van den Dool et al. 1991). Intercomparisons between the model results and the observed data, as well as between positive and negative LFAs, were examined in detail. After a brief description of the GCM integrations and the observational data in section 2, comparisons of variance and skewness characteristics will be shown in section 3. The geographical distribution of the positive/negative large anomalies, as well as their associated circulation patterns, will be presented in some detail in section 4. Issues regarding persistent anomaly regimes versus short, but frequently occurring, anomalies will be presented in section 5. A brief discussion concerning a coherent relationship between the principal storm tracks, the mean flow, and the low-frequency anomalies will be given in section 6, and conclusions in section 7.

2. GCM runs and NMC analyses

The general circulation model employed is a T40 version of the global spectral model used operationally at NMC, in 1990, for medium range weather forecasting. The model has 18 vertical levels in sigma coordinates. A complete documentation can be found in Sela (1980) with updates of the model by Kanamitsu (1989) and Kalnay et al. (1990). This model was integrated for 10 years (3653 days), starting from the initial conditions on 31 July 1990. The external boundary conditions were as follows: Solar radiation was updated every day according to the astronomical calendar. The snow depth, soil moisture, and sea ice and sea surface temperature were updated every day according to their known climatologies. Some particular aspects of the climate of this 10-year integration can be found in Van den Dool et al. (1991), Van den Dool (1991a), Van den Dool and Saha (1993), and Anderson (1993).

In this study, the geopotential heights at 500-mb level (Z500) during northern winter season (1 November–31 March) were examined. The 10-year daily climatology (smoothed) was first subtracted from each daily Z500 field. Then, an 11-day running mean low-pass temporal filter was applied to suppress the synoptic-scale high-frequency components of the fluctuations.

The NMC operational analysis was used to represent the characteristics of the real atmosphere. The observed data (the analyses) and their documentation have been prepared and made readily available to the scientific community on a compact disk by the joint effort of the Department of Atmospheric Sciences, University of Washington and the Data Support Section, National Center of Atmospheric Research. The NMC analyses from 1957/58 winter through 1988/89 winter were used in this study. Missing analyses were filled in with linear interpolations. If the missing analyses were longer than three consecutive days, the entire winter was excluded from our present comparisons. Specifically, 1961/62, 1962/63, 1980/81, and 1981/82 winters were not used. The remaining 28 winters of Z500 analyses were then treated as follows: 28-year daily cli-

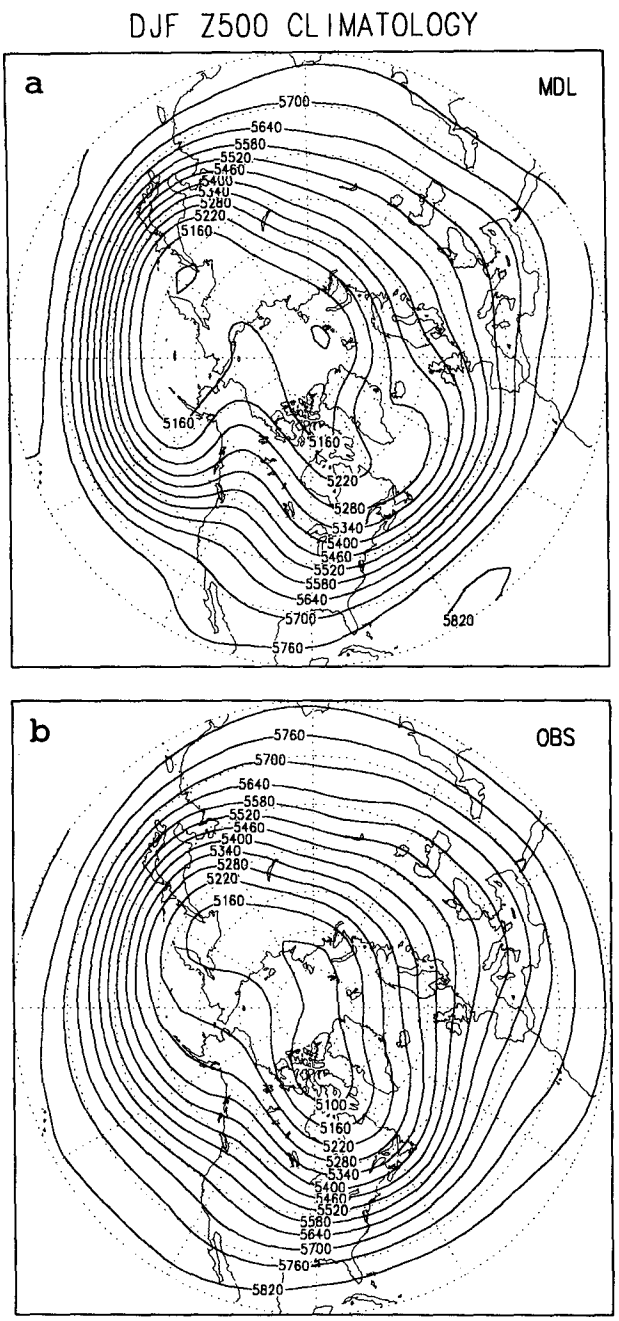

FIG. 1. The Dec–Jan–Feb Z500 climatology. Ten-season mean for MDL runs, 28-season mean for OBS data.

matology (smoothed) was removed first, then the anomalies were low-pass filtered by an 11-day running mean.

3. Mean, variance, and skewness

Figure 1 compares the winter (DJF) climatology of the MRF model and reality. In general, the model simulation is fairly good, with mean troughs over the eastern continents/western oceans and a mean ridge over western North America and much of Eurasia. The model does show a stronger stationary wave pattern. Also, heights are simulated too low over the lower latitudes and too high over the polar region. For better comparison of the stationary waves, Fig. 2 presents another view of the DJF climatology by subtracting its respective zonal mean. Compared with the observations, the model's North Pacific trough is seen to be

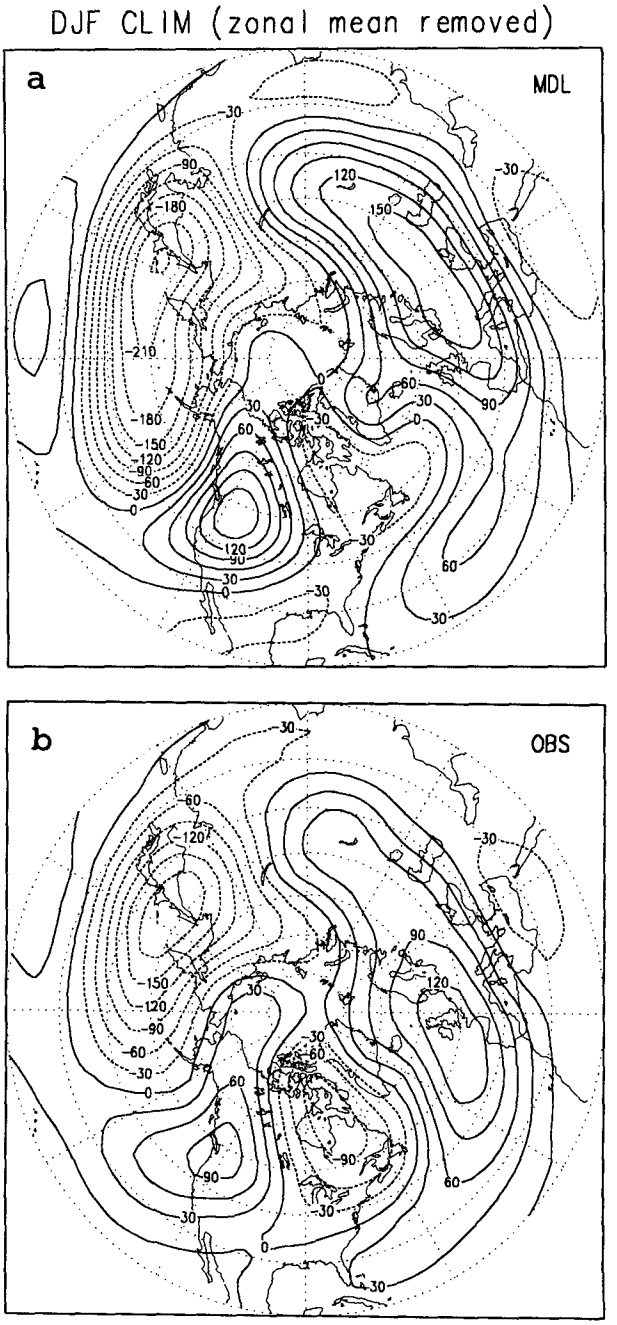

FIG. 2. Same as Fig. 1 except with subtraction of the zonal means.

deeper and extends much more toward the eastern Pacific. The model North America ridge is seen to be much stronger, while the northeast American trough is much weaker. Over Europe, the model shows the ridge extending much farther into Eurasia, whereas the real atmosphere shows its main center over the eastern North Atlantic.

Figure 3 compares the geographical distribution of standard deviation (SD) of the model and the observations. The first contour shown is 60 m for the MDL runs (Fig. 3a) and 80 m for the observed data (Fig. 3b). The model's SD is, therefore, much weaker, a well-known deficiency of most GCM simulations. The geographical patterns do show a broad similarity. Careful comparisons between variance maxima (Fig. 3c) reveal, however, some critical discrepancies that imply a rather different regional climate. In Fig. 3c, the shaded areas are for MDL SD larger than 80 m, whereas unshaded contours are those of the OBS SD with values larger than 120 m. Over the North Pacific, the MDL SD maximum is much closer to the coast of North America, about 1500 miles east of the OBS SD. Over the North Atlantic, the MDL SD maximum is also much farther southeastward of the OBS SD maximum. Over both regions, the MDL SDs are much weaker than those of the OBS, as is the SD over Baffin Island (80 vs 120 m). The MDL variance over the Siberian Arctic is however more comparable and the location is near perfect. Over the North Atlantic, the MDL tends to develop widely separated SD maxima, one over Baffin Island, another over the eastern Atlantic, whereas the OBS has its large SDs in between.

Recently Barnston and Van den Dool (1993) documented the standard deviation of monthly mean 700-mb geopotential heights for each of the 12 months over the 1950–1991 period. Their results indicate that the position of the SD maxima over the northern oceans remains rather stationary throughout the year. Considering the small seasonality of the observed SD field, the positional differences between Figs. 3a and 3b are substantial. They are as different as winter and summer fields.

We would like to know whether the positive or negative anomalies contribute most to the variance maxima. Or maybe the frequency distribution is rather symmetric as one would expect from a linear dynamical system. Furthermore, is there any difference in the composition of the North Pacific and Atlantic variance maxima? Figure 4 displays two frequency distributions of the OBS low-frequency anomalies (LFAs) over the North Pacific maximum SD area. The unit along the ordinate is "number of days." The anomaly interval used in the frequency tallies is 30 m. The integrated sum under each curve is (141 × 28) 3948 days. The frequency distributions at 45°N (southern flank of the SD maximum) are nearly symmetrical in shape (lower panel), whereas the distributions at 55°N (northern flank of the SD maximum) are enormously positively

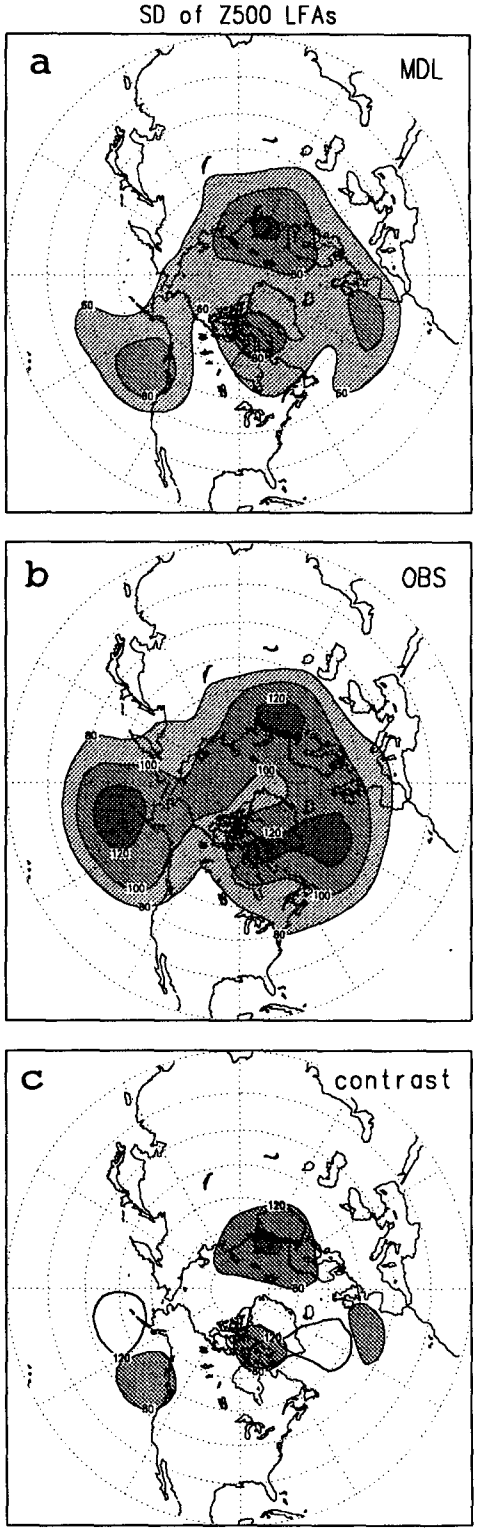

FIG. 3. Wintertime standard deviation of 11-day running mean filtered Z500 anomalies. For (a) 10-year MDL runs and (b) 28-year NMC analyses. Shading/contour interval is 20 m. In (c), the variance maxima are compared in the same graph; the first shading/contour is 80 m for MDL and 120 m for OBS.

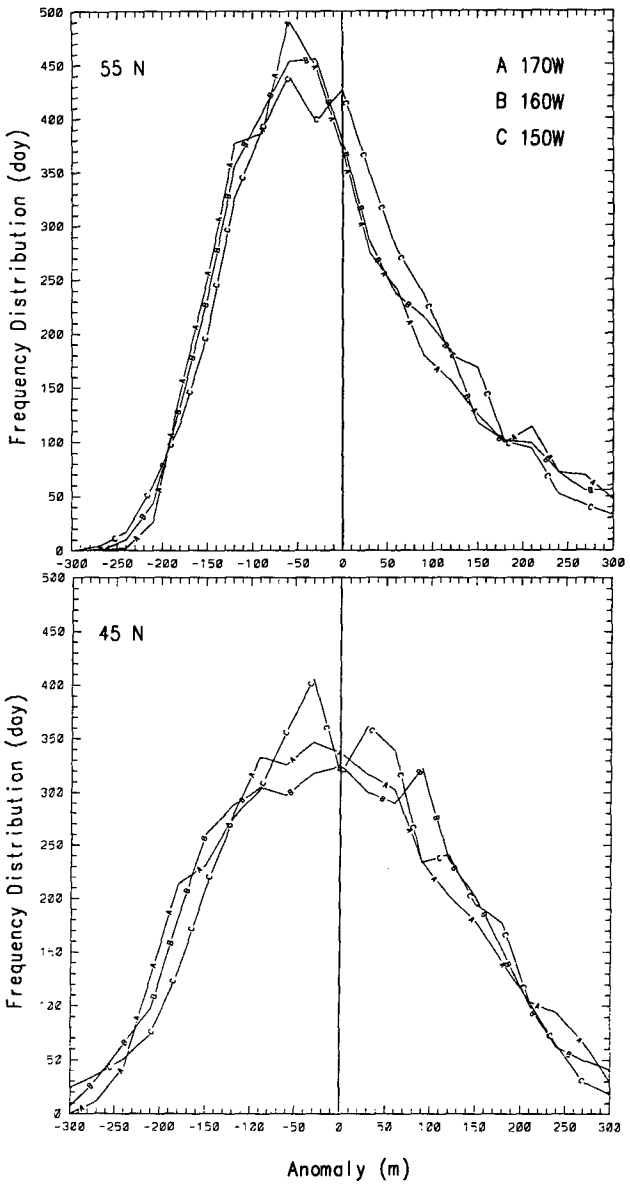

FIG. 4. Frequency distribution of the observed wintertime Z500 LFAs over the North Pacific. The grid point for each of the three curves is indicated in the figure.

skewed (upper panel). This can be seen especially when focusing on the large anomalies, say those exceeding 200 m. Negative anomalies of that magnitude rarely occur, whereas positive anomalies show up a significant percentage of the time. Figure 5 presents a similar display for the North Atlantic maximum SD area. Here, the frequency distributions at 60°N (northern flank of the SD maximum) are also positively skewed (upper panel); however, the distributions at 50°N (southern flank of the SD maximum) show instead a negative skewness (lower panel). The chance of developing large anomalies of the same sign near the center of the maximum SD area in the northern oceans is, therefore, not equal. Both Pacific and Atlantic maximum SD areas are known to be near the exit of their respective principal storm tracks. Yet, the frequency distribution of the LFAs exhibit somewhat different characteristics from each other. We wonder whether the physical processes leading to the development of, say, blocking highs may be the same for these blocking flow prone areas.

To obtain an overall comparison of the geographical distribution of the skewness between the model and the observed atmosphere, the skewness of the Z500 LFAs was obtained for each grid point and compared in Fig. 6. The coefficient of skewness is defined as the

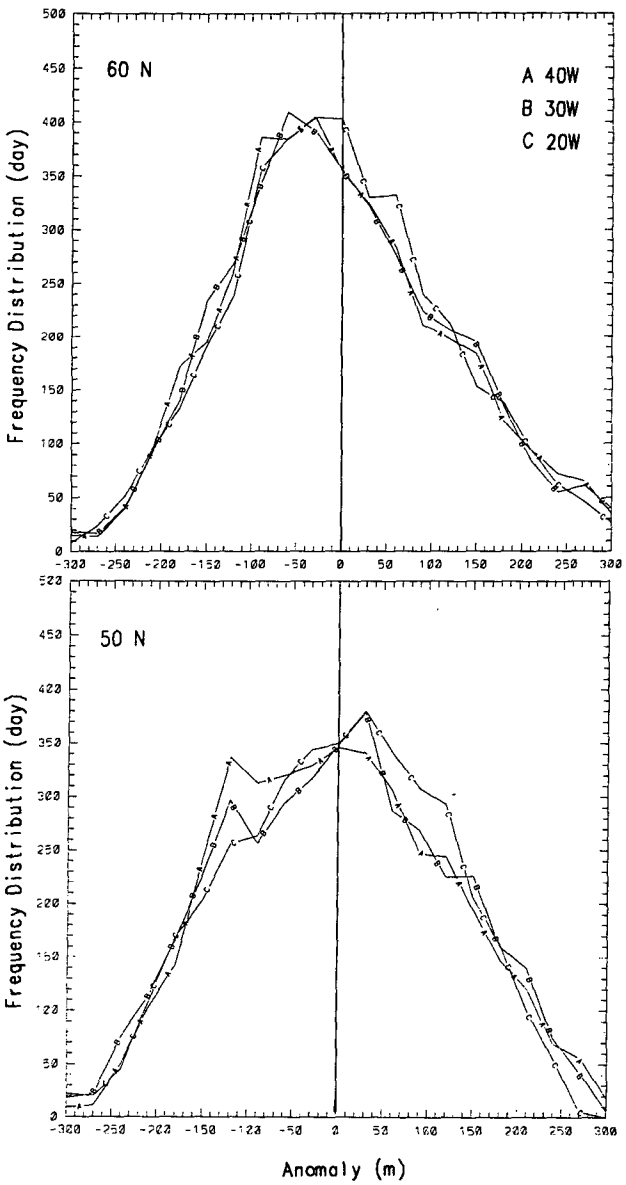

FIG. 5. Same as Fig. 4 except for the region over the North Atlantic.

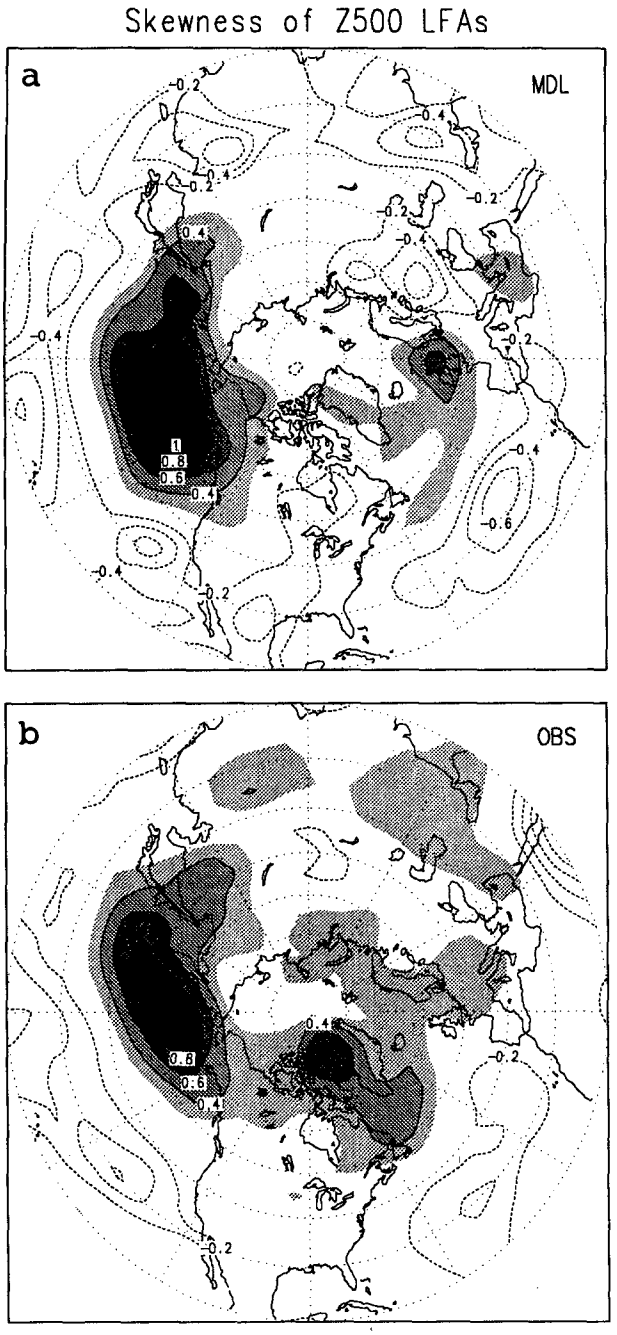

FIG. 6. Coefficient of skewness of the wintertime Z500 LFAs (a) for MDL runs and (b) for OBS data. Shading/contour interval is 0.2; first shading begins at 0.2.

normalized third moment of the fluctuations about the mean (e.g., White 1980). As shown in the figure, positive skewness is, in general, found north of the jet stream latitudes and negative south of them, agreeing with White (1980), although his results were for daily data, and Van den Dool (1991b) and Nakamura and Wallace (1991), although their results had been filtered differently. Detailed comparisons between the model (Fig. 6a) and the observed (Fig. 6b) distributions reveal substantial differences: much larger and wider domain of positive skewness for the model over the North Pacific as well as over the eastern North Atlantic. On the other hand, large positive skewness for the observed extends from Baffin Bay southward through the Davis Strait to the Labrador Sea, while the model does not have much of either positive or negative skewness over that region. Therefore, the preferred locations for large positive/negative anomalies appear to be different between the model and the real atmosphere. Further study should be made to find out how different the model's circulation patterns are from the real atmosphere.

4. Large anomalies and associated circulation patterns

a. Observed low-frequency anomalies

In this subsection we would like to determine further how the observed large LFAs are distributed geographically. Will the large negative anomalies be located in the same areas as the large positive anomalies? Do the large anomalies determine much of the spatial distribution of variance (Fig. 3) and skewness (Fig. 6)?

From the frequency distributions in Figs. 4 and 5 we see that there are quite a few positive and negative anomalies exceeding 200 m in magnitude. We therefore select 200 m as the threshold level to isolate the desired large anomalies. Figure 7a presents the percentage of time during 3948 winter days that the positive anomalies exceed 200 m, and Fig. 7b those negative anomalies exceeding −200 m. The contour interval is 2% (in unit of percentage of time; 1% = 39.48 days). The first contour is also 2%. Substantial differences in geographical distribution can be seen in the OBS data. Positive anomalies exceeding 200 m occur up to 8% of the time in the North Pacific, whereas negative anomalies exceeding −200 m occur only up to 4% of the time. A similar skewness can be observed over the North Atlantic, Davis Strait, as well as over northern Siberia. For a sharper contrast, Fig. 7c superimposes both positive and negative large anomalies on the same map. To avoid overcrowding, only values of 4% and above are compared. The negative LFAs are shaded and the positive contoured. Spatially distinct distributions can now be observed. Besides large differences in frequency, the negative LFAs are seen to develop preferably over the southern flank of the positive LFAs.

When comparing Fig. 7 to Fig. 3b, it is clear that the large anomalies, such as those exceeding 200 m, explain almost completely the spatial pattern of the standard deviation, in excellent agreement with the recent findings of Nakamura and Wallace (1991) and Yang and Reinhold (1991). In this article we show further that the low-frequency variance over the North Pacific, North Atlantic, and northern Siberia is due mostly to large positive anomalies.

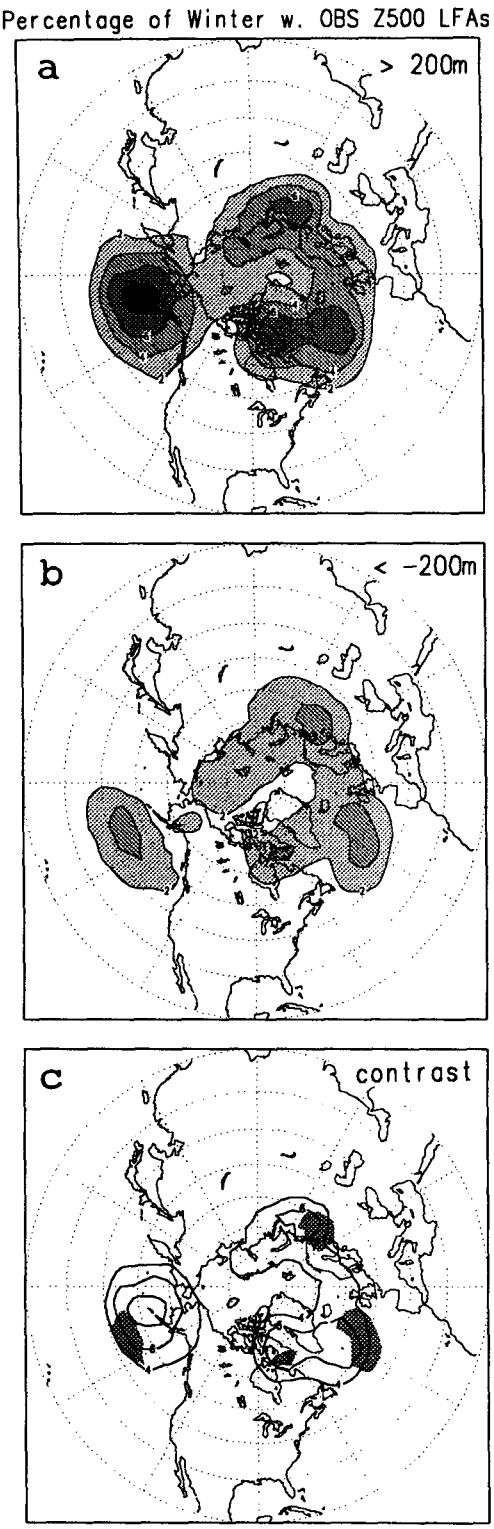

FIG. 7. Percentage of time during 3948 wintertime days that the observed (a) positive LFA exceeds 200 m, (b) negative LFA exceeds −200 m. Contour interval is 2% (equal to 79 days). For (c), contrast superposition, the first shading/contour is 4%.

b. Large anomalies in GCM runs

The wintertime LFAs of the MDL data are next analyzed for the large positive and negative anomalies, separately. Recall that the model's amplitude of disturbances is much smaller than the observed. We therefore reduce the threshold level from 200 m for the OBS to 150 m for the MDL. Figure 8 presents the geographical distributions of the percentage of time during 1510 winter days when the positive LFAs exceed 150 m (Fig. 8a), and the negative LFAs exceed −150 m (Fig. 8b). Over the eastern North Pacific, large positive LFAs develop twice as frequently as the large negative LFAs (8% versus 4%), an occurrence ratio similar to that of the observed. However, the frequency of occurrence of large positive and negative LFAs are about the same over the eastern North Atlantic and the Davis Strait areas, unlike those observed for these regions. Large negative LFAs are much more frequent and widespread than large positive LFAs over northern Siberia. This is contrary to observations.

Comparing Fig. 8 to Fig. 3a, we notice again that the large anomalies explain almost completely the standard deviation, just as in the OBS data. However, the variance maxima over the eastern North Pacific are mostly due to the large positive anomalies. On the other hand, the variance maximum over northern Siberia is due mostly to the large negative anomalies. Over the North Atlantic and Baffin Bay/Davis Strait area, both polarities contribute to the low-frequency variances.

c. MDL runs versus OBS data

In this subsection the large LFAs of the GCM runs and the observed data are placed on the same map so that distinct differences will be easily detected. Figure 9 presents the superposition of the large positive LFAs. Those of the MDL runs are shaded and those of the observed are contoured. The first shading/contour is 4% and the interval is 2%. The LFAs are those exceeding 200 m for the observed and 150 m for the MDL runs. As seen, the MDL runs are capable of producing large positive LFAs at three of the four major variance areas (i.e., North Pacific, Davis Strait, and northern Siberia), although they never overlap completely with the observed. Note that the positive LFAs in the MDL runs in the North Pacific are about 1500 miles southeast of the OBS LFAs. Another substantial deficiency of the model can be found over the North Atlantic where positive LFAs occur frequently in the OBS data but are absent in the MDL data.

Figure 10 presents the superposition of large negative LFAs. Because negative LFAs occur less frequently than positive LFAs, the contour/shading in this figure starts at 2% instead of 4% as used in the previous figure. The interval for both shading and contour remains 2%. Over the North Pacific, the MDL LFA center is again about 1500 miles east of the OBS LFA center. Over

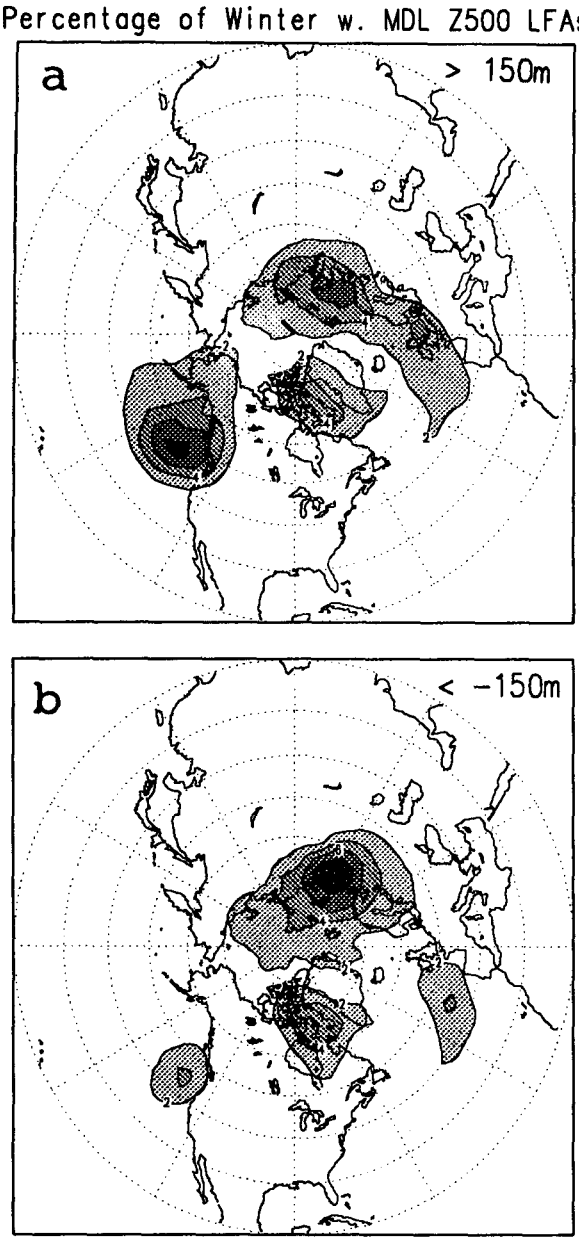

FIG. 8. Percentage of time during 1510 wintertime days that the MDL (a) positive LFA exceeds 150 m (b) negative LFA exceeds −150 m. Contours and shadings are the same as those of Fig. 7.

the North Atlantic, the MDL center is clearly located south of the OBS. Another substantial difference can be found over northern Siberia: instead of much weaker presence, the MDL LFAs develop twice as frequently as the OBS LFAs, 8% versus 4% of the wintertime.

d. Circulation patterns associated with MDL/OBS LFAs

Large differences in model and observed short-term climate can be inferred further from their LFA associated circulation patterns. From Figs. 9 and 10, four major centers can be identified where large positive/negative LFAs most frequently developed. They are over the North Pacific, North Atlantic, Davis Strait,

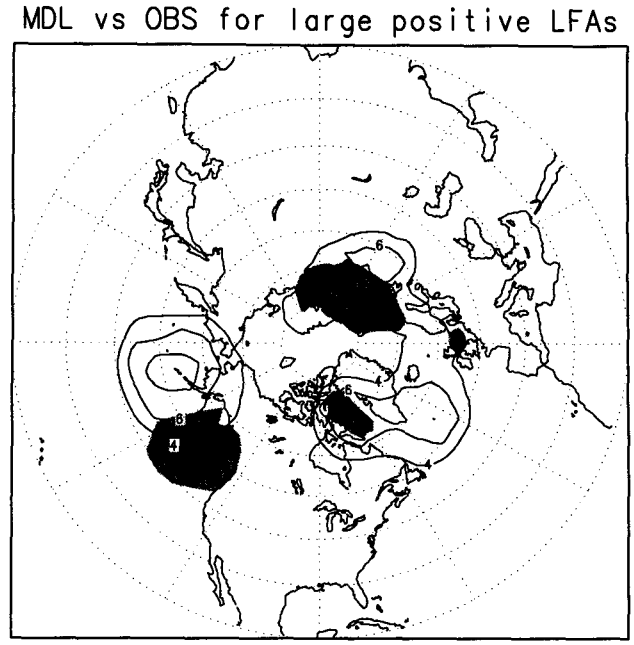

FIG. 9. Superposition of Figs. 7a and 8a for better contrasting. Shading/contour interval is 2%, but the first shading/contour is 4%. Recall that the threshold is 200 m for the OBS data but only 150 m for the MDL runs.

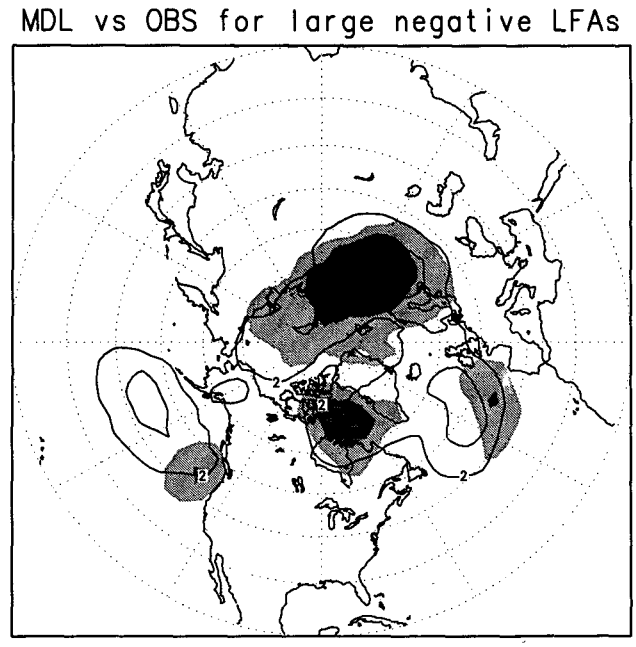

FIG. 10. Same as Fig. 9 except for the contrasting of the large negative LFAs.

and northern Siberia. Based on each LFA center, circulation composites can be constructed by averaging over those cases with LFA exceeding the threshold level.

Figure 11 compares the composite circulation patterns for the North Pacific LFA centers. The model's "wavetrains" (the left panels) appear to be short and aligned in a zonal direction, whereas the observed wavetrains (the right panels) consist of four centers and assume a giant arch on the sphere, similar to the observed Pacific/North America teleconnection pattern (e.g., Barnston and Livezey 1987).

If we focus our attention to the OBS composites only, we can also notice certain subtle differences between the positive and the negative composite. The positive-center-based wave train (the upper panel) displays more southward downstream teleconnection. The wavetrain also has a stronger north–south dipole contrast over the North Pacific.

Figure 12 compares the composite circulation patterns for the North Atlantic LFA centers. For the positive-center-associated composites (the upper panels), the observed circulation displays a NAO pattern [North Atlantic Oscillation, e.g., Barnston and Livezey (1987)] over the North Atlantic, whereas the model yields instead a blocking anticyclone over the British Isles. For the negative-center-associated composites (the lower panels), the most dominant OBS circulation pattern is a deep trough over the North Atlantic surrounded by weak positive anomalous heights except for the immediate upstream, whereas the MDL composite tends to have a clear upstream train of waves over the North Pacific/North America sector.

Comparing the most dominant circulation patterns in the model, a clearly distinguishable feature can be identified: an anticyclone over the British Isles versus a major trough over the North Atlantic, which is about 1000 miles southwest of its positive counterpart and is teleconnected with an upstream wavetrain, as described above. If a linear analysis tool, such as an empirical orthogonal function (EOF) analysis, were used to extract the most dominant mode of the model's circulation patterns, the result over the North Atlantic will be surely quite different from what we have seen in this figure: instead of two distinguishable circulation patterns, the EOF analysis will yield only a single dominant pattern with center located perhaps 500 miles south of the British Isles.

5. Persistent versus frequently occurring anomalies

As mentioned in the introduction, one of our primary interests in this 10-yr GCM run is to find out whether the MRF model is capable of creating and subsequently maintaining the large LFAs as long as those observed in the real atmosphere. The results shown in the previous figures cannot distinguish persistent anomalies from less persistent but frequently occurring ones. In this section, we will isolate, for every grid point, the longest lasting of all of the LFAs with amplitude exceeding the chosen threshold, and also determine the average "duration of persistence" of all LFAs.

Figure 13 presents and compares the longest persistent event at each grid point. The shaded areas represent persistence lasting longer than 10 days. The contour/shading increment is 5 days. Comparing the model (the left panels) and the observed results (the right panels), we see that the model is able to maintain large LFAs at a few locations: for positive LFAs, the eastern North Pacific for as long as 30 days, and western Europe as long as 15 days. In general, the model does not maintain a positive large LFA as long as the real atmosphere except in the eastern North Pacific. Over the North Atlantic, for instance, while the observed shows persistence longer than 20 days for a wide area, and even 30 days for some, the model shows a much smaller area with only 10 days persistence. Most remarkable is the contrast for the negative LFA persistence over the North Pacific (the lower panels). While the observed shows persistence longer than 30 days for a large domain, the model shows only persistence beyond 10 days in an area near the coast. The model does show much longer persistence of negative LFAs over the eastern North Atlantic, 20 days versus about 10 days for the observed. The model also shows longer persistence for the negative large LFAs over Baffin Island and the Siberian Arctic.

In succinct form, the model is able to maintain long-lasting large positive/negative LFAs over the eastern oceans near the coast, where the real atmosphere may or may not have long-lasting LFAs. In most other areas, the model does not maintain the large LFAs as long as the observed except for Baffin Bay and the Siberian Arctic areas.

It is remarkable to note that, over the eastern North Pacific, while the OBS negative LFAs may persist much longer than the positive ones (40 days vs 20 days), the MDL LFAs display an opposite behavior, with the negative LFAs persisting much less than the positive ones (10 days vs 30 days).

The average duration of persistence is shown in Fig. 14, with a first contour of only 5 days. In general, both MDL and OBS LFAs display similar average duration of LFA events, about 5–10 days. However, over the North Pacific, the MDL shows two small areas with average persistence a little beyond 10 days. When comparing with the previous figure, it implies that such a long-lasting event occurred only once during the entire 10 years. Near the Seattle/Vancouver area, the MDL negative LFA events with duration of about 10 days appeared only twice in 10 years. The OBS large LFA events, in comparison, are much more frequent south of the Aleutians.

6. Discussion

Distinct weather regimes can develop within even a single season and result in short-term climate change.

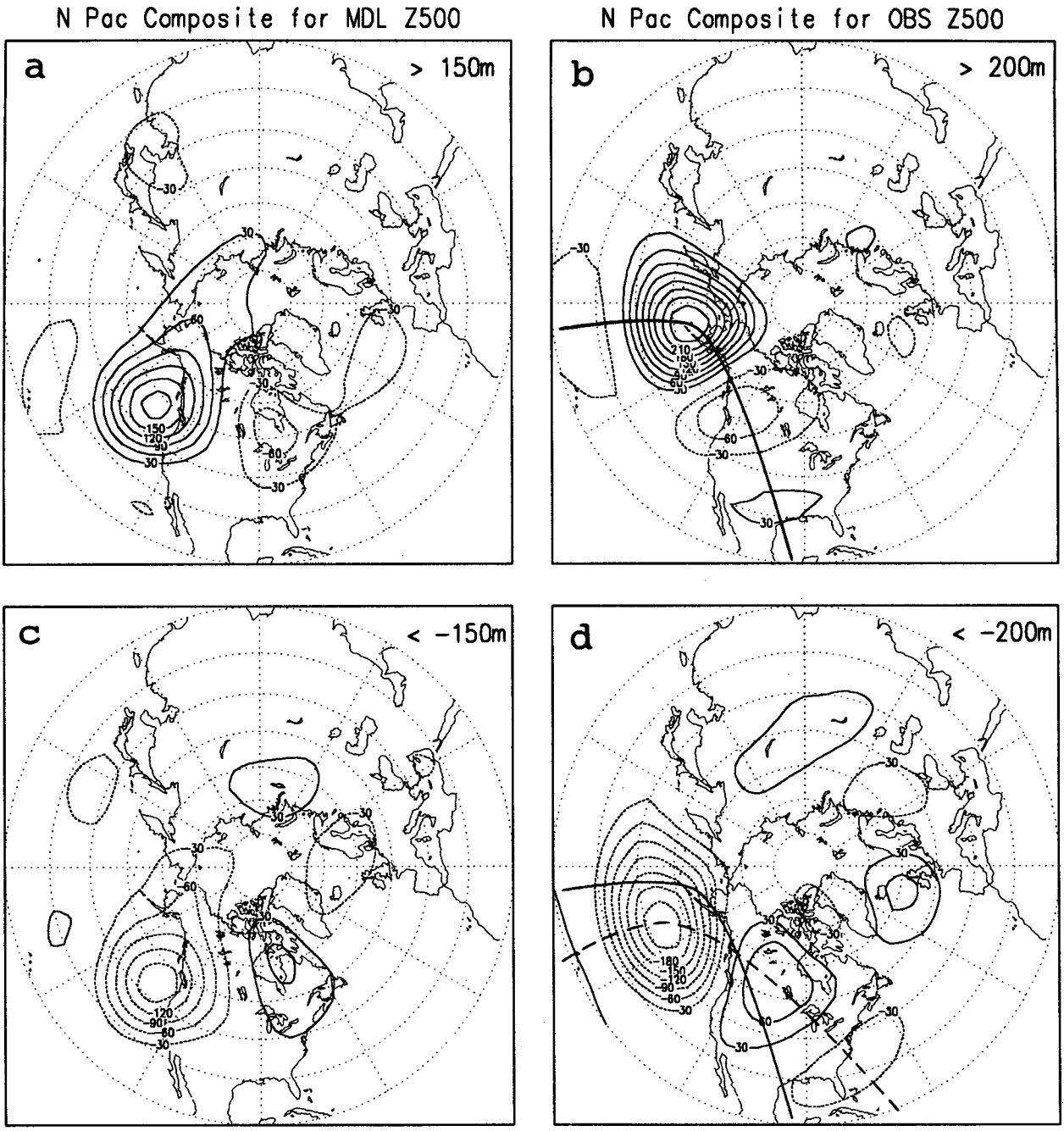

FIG. 11. Composite circulation patterns based on the LFA variance centers over the North Pacific. Left panels for MDL runs, right panels for OBS data. Upper panel for those based on the positive LFA centers and lower panels for those based on the negative LFA centers.

The capability of a GCM to correctly simulate the persistent weather events is a necessary condition for a successful short-term climate prediction. Current GCM forecast skill often depends upon the prevailing circulation regimes. Accurately predicting regime transitions will continue to be a major challenge (e.g., Chen and Van den Dool 1995). The following comparisons can probably exemplify the capability and the deficiency of the MRF model used in this study.

The persistence of a strong atmospheric blocking dipole observed over the North Atlantic on 20 January 1987 is shown in the left panels of Fig. 15. Once established, this block persisted for a 12-day period. A subjective search for the same kind of flow regime in the 10-yr model run was conducted and the case with closest resemblance is identified and shown in the right panels of the figure. The MRF model does have the capability of generating and maintaining a long-lasting

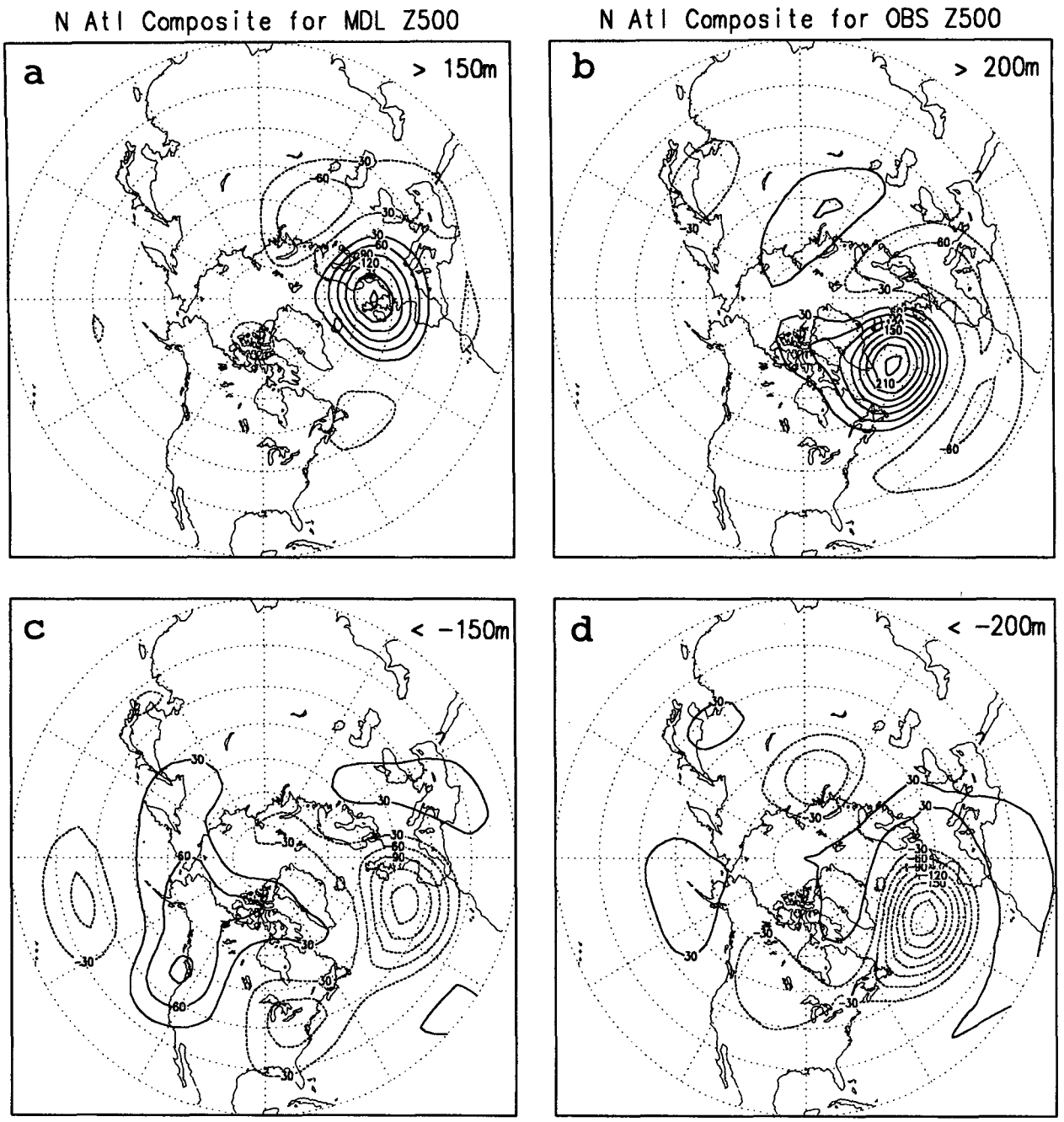

FIG. 12. Same as Fig. 11 except for patterns based on the LFA variance centers over the North Atlantic.

blocking-like flow. However, careful examination reveals that the model circulation behaves more like a persistent anomalous ridge rather than a blocking dipole: the positive anomaly is at least 10° south of the atmospheric blocking anticyclone, and the companion negative anomalous height south of the block is absent from the model circulation. Aside from much weaker anomalies, the model flow configuration is clearly different from that of the real atmosphere. The regional short-term climate would subsequently not be the same.

The lack of a similar blocking flow regime in 10 years of integration suggests that the model considered here generates substantially different short-term climate anomalies from those of the real atmosphere. It appears that this model is equipped with sufficient dynamics to generate large and persistent weather regimes. However, the model is deficient in simulating the amplitude

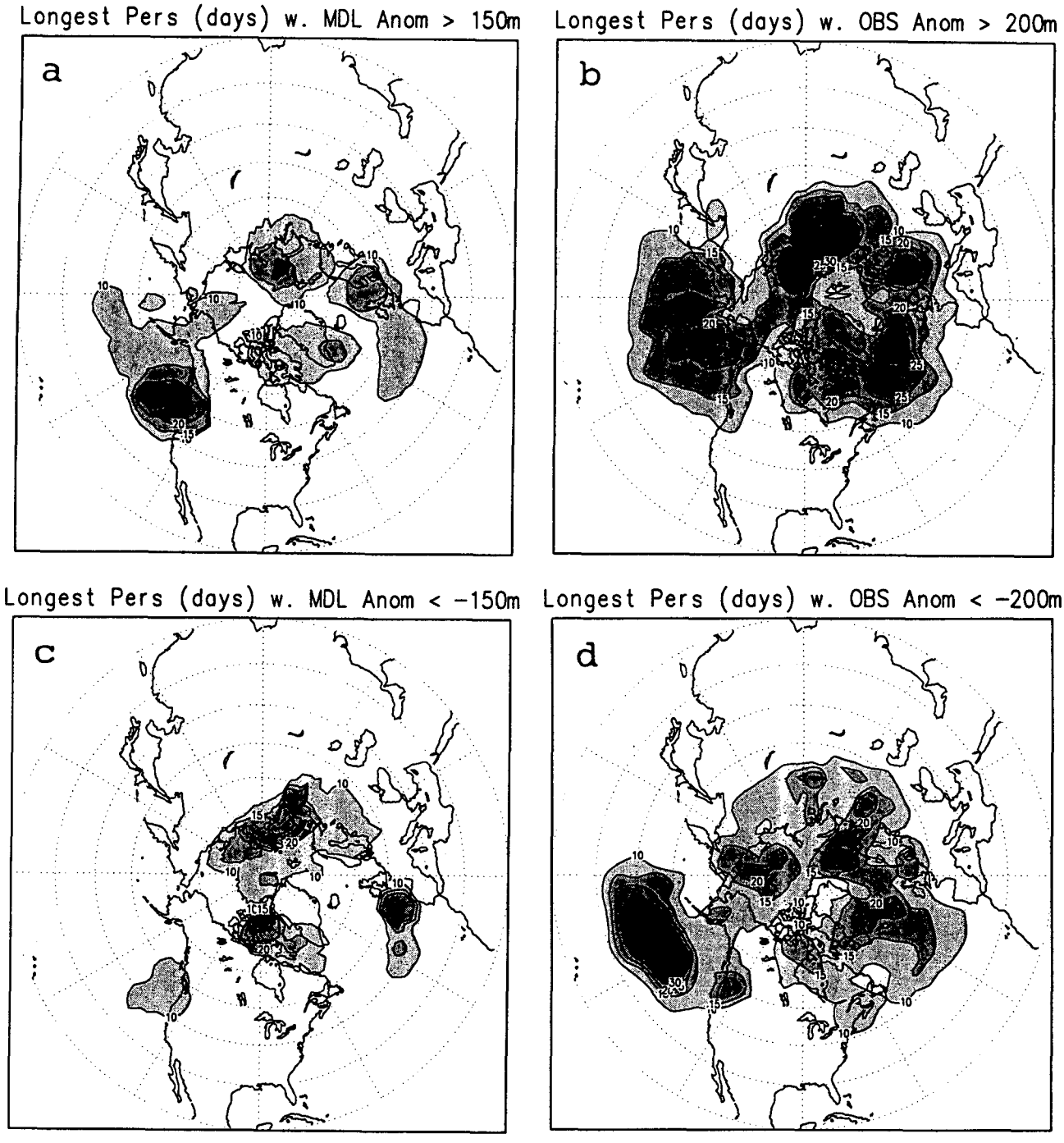

FIG. 13. The longest persistence (in unit of day) experienced during the period considered with amplitude exceeding the chosen threshold. Left panels for MDL runs, right panels for OBS data; upper panels for positive LFAs, lower panels for negative LFAs. The first shading/contour is 10 days and the interval is 5 days.

and location of these large LFAs. Correct simulation of these features is a necessary condition for the skillful prediction of short-term climate. This is, indeed, a very challenging practical problem.

It is known that a blocking high prefers to develop at the exit of the principal storm tracks. The present model indicates a preferred location for large positive LFA development far southeast of those of the observed. This probably suggests that the MDL's principal storm tracks do not exit in the same regions as observed over both the North Pacific and the Atlantic Oceans. To verify this suspicion, the synoptic-scale fluctuations

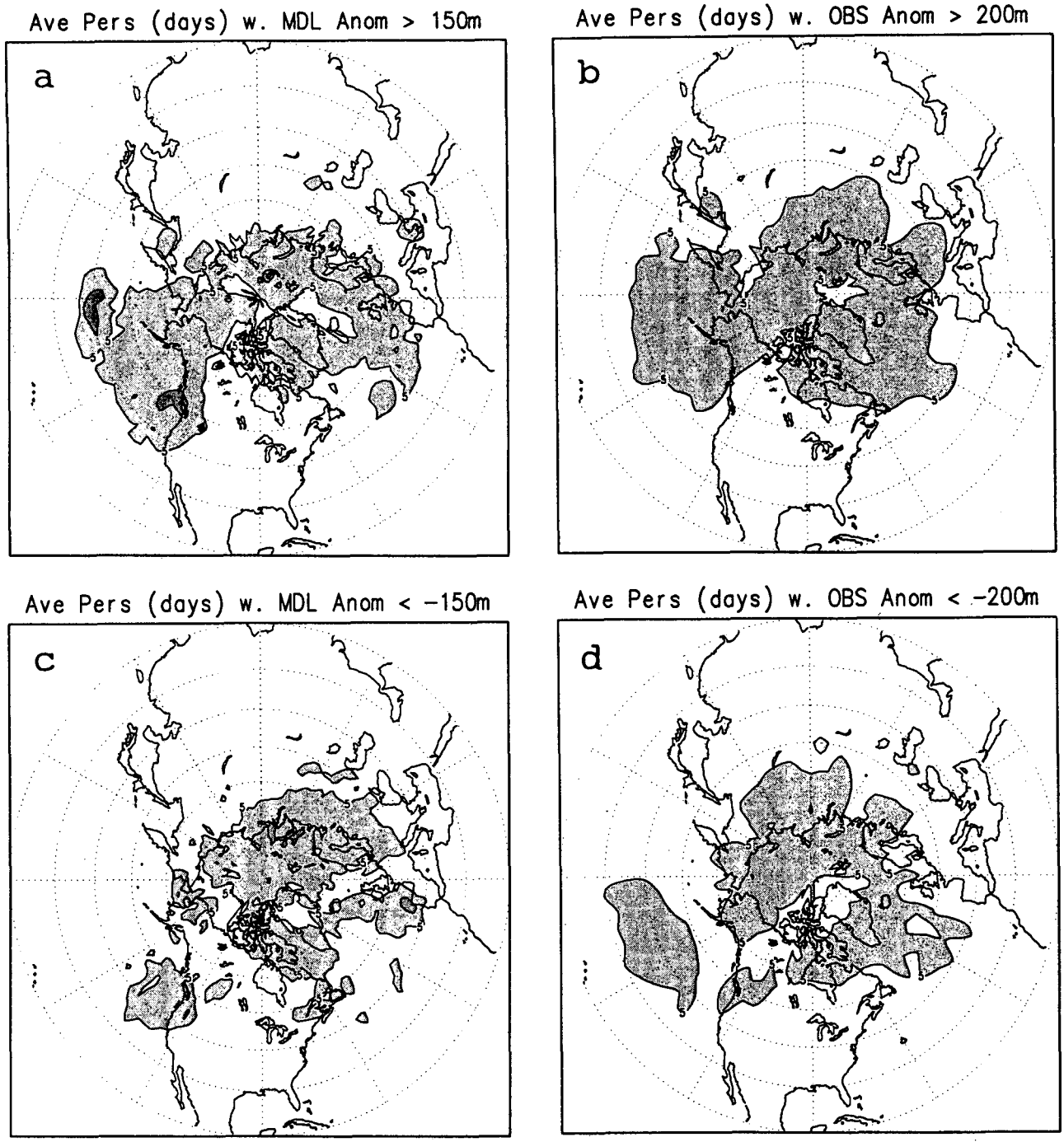

FIG. 14. Same as Fig. 13 except for the average duration with LFA exceeding the chosen threshold.

were investigated for both the MDL runs and the OBS data. For this purpose, a high-pass 7-day running mean filter was applied to both MDL and OBS time series at each grid point to remove the low-frequency components and to isolate the synoptic-scale disturbances. The resulting high-passed Z500 fluctuations were then used to obtain the standard deviation at each grid point.

As shown in Fig. 16, although the principal storm tracks of MDL and OBS appear to be similar at first sight, careful examination reveals that the observed storm tracks (Fig. 16b) tend to be heading toward the Gulf of Alaska over the North Pacific and the region between Iceland and the British Isles over the North Atlantic, whereas in both regions the MDL storm tracks (Fig.

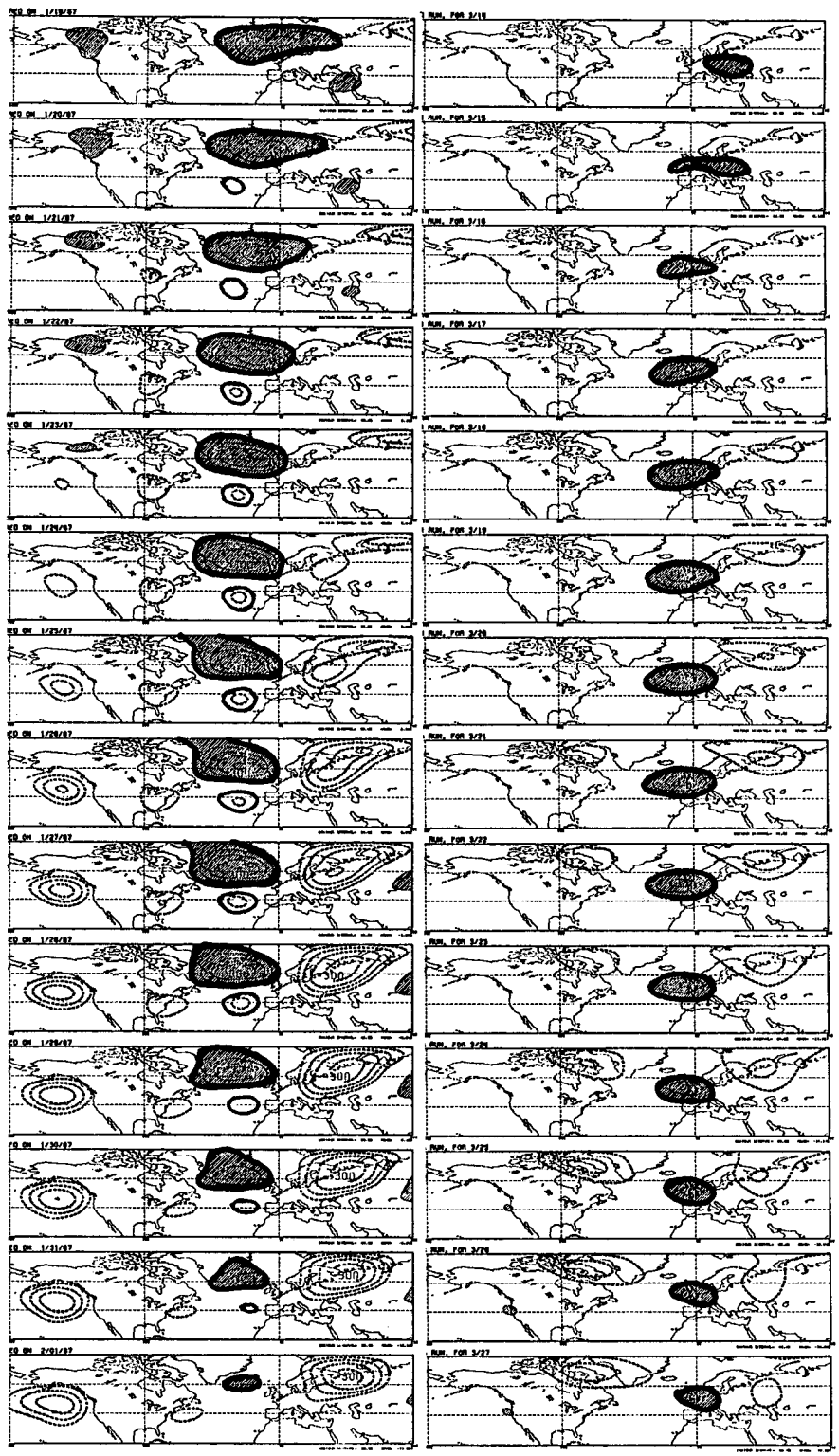

FIG. 15. Evolutions of the 11-day running mean filtered LFAs during 14 consecutive days. Positive anomalies exceeding 120 m are shaded and negative anomalies less than 120 m are contoured with dashed curves. The contour interval is 60 m. The left panels are OBS data, and the right panels are MDL runs.

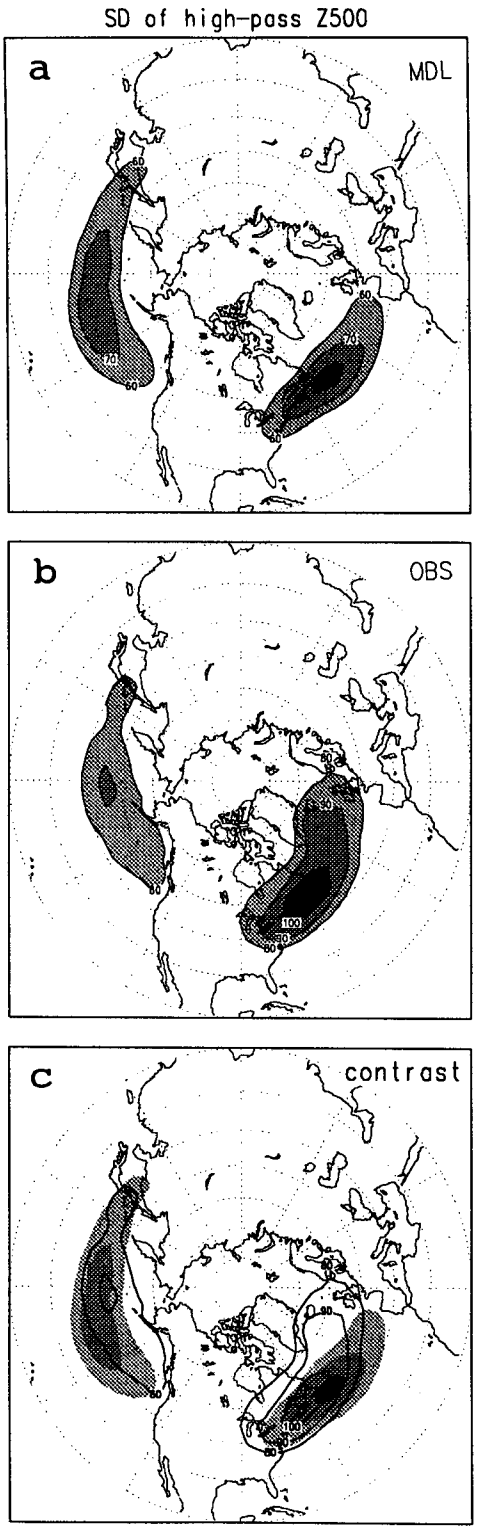

FIG. 16. The standard deviations of the high-pass Z500 synoptic-scale disturbances (a) for 10-yr MDL runs and (b) for 28-yr NMC analyses. First shading/contour is 60 m for the MDL runs and 80 m for the OBS data. Interval is 10 m.

16a) tend to exit farther south than observed. Figure 16c displays the superposition, where the shaded areas represent the MDL high-pass SDs and the contours the OBS ones. Note that the contour starts at 80 m, but the shading starts at 60 m. The MDL high-pass SD is smaller than the observed, as expected. The equatorward displacements at the exit of the MDL storm tracks can be clearly seen, especially over the eastern North Atlantic.

The December through February mean zonal wind at the 250-mb level (DJF U250) was also obtained and compared in Fig. 17. The eastward extension of the MDL jet stream can be clearly seen. The southward shift of the MDL mean jet is also noticeable over the western North Atlantic. These results are consistent with those shown in Figs. 9 and 15 where the locations of the large positive LFAs between MDL and OBS were contrasted.

The issue of reproducibility of the above results was examined by dividing the total amount of data into two equal parts and repeating the calculations. Ten years of the model runs and 28 years of the observed data were found sufficient to offer a rather stable picture as reported: the model results were nearly indistinguishable between the two 5-yr samples, and the two portions of observed data showed only minor differences.

Another issue is the lower boundary. The sea surface temperature (SST) used in this study, although containing an annual cycle, does not have the interannual variation. The impact of the tropical heating anomalies on the general circulation in the midlatitudes has been a major concern (e.g., Wallace and Blackmon 1983) but cannot be demonstrated in this study. For that purpose, another 10-yr MRF integration was conducted with prescribed actual SST variations. This long integration was completed recently. The potential effect of the SST anomalies will be addressed with this new dataset in a forthcoming investigation.

7. Conclusions

A T40 version of the NMC MRF model was employed to obtain simulated meteorological data for 10 continuous years. Wintertime Z500 fields were analyzed to determine the model's capability of generating persistent short-term climate anomalies. Temporal filtering by an 11-day running mean was applied to obtain the low-frequency components of the model's variability.

The climatology of the Z500 mean height of the model run resembles the observed fairly well, with the model's amplitude of its stationary waves somewhat larger. However, comparison of the geographical distributions of the low-frequency variance indicates that, in addition to smaller magnitude, the model tends to misplace its variance maxima about 1500 miles farther east over the North Pacific and farther southeast over the North Atlantic.

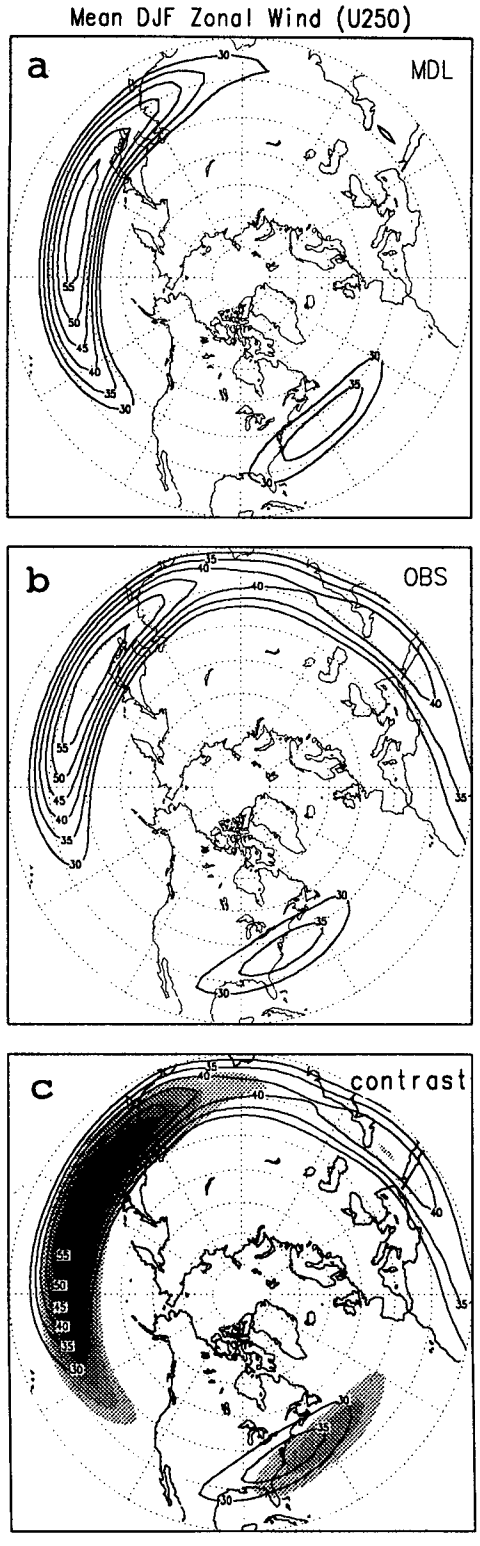

FIG. 17. The Dec–Jan–Feb mean zonal wind at 250-mb level. First shading/contour begins at 30 m s^{-1} with increment of 5 m s^{-1}.

Since the frequency distribution of the LFAs are highly skewed, investigations were conducted separately for the positive and negative large-amplitude LFAs. Amplitude thresholds of 200 m for the OBS data and 150 m for the MDL runs were applied to extract the large-amplitude LFAs. The thresholds used were found to be suitable for isolating the most persistent anomalies in both the model and real atmosphere. Four-way comparisons among MDL runs, OBS data, positive, and negative LFAs were examined. For large positive LFAs, the model and the observed have comparable probability of occurrence over the North Pacific and North Siberia. But, over the North Atlantic, the model displays little chance of occurrence (Fig. 9). For large negative LFAs, the model's occurrence percentage is only half as much as that observed (2% vs 4%) over both the North Pacific and North Atlantic. However, over North Siberia, the model shows twice as frequent (8% vs 4%) as that observed (Fig. 10).

Over the northern oceans, the model's positive/negative LFAs are frequently about 1500 miles too far east or southeast. As a consequence, their respectively associated circulation patterns are substantially different from that observed. For instance, over the North Pacific, the real atmospheric pattern displays a giant Pacific/North America wavetrain, while the model yields only a short and more or less zonally oriented oscillation (Fig. 11). Because of the large skewness in the distribution of large LFAs, separate analysis on positive and negative anomalies can sometimes result in clearly distinguishable circulation patterns that cannot possibly be identified if a linear analysis tool, such as an empirical orthogonal analysis, is used to extract the most dominant mode of the circulations.

The NMC MRF model does have the capability of generating long-lasting weather anomalies, especially over the northeastern oceans and the adjacent western continents (Fig. 13), where the real atmosphere, however, may not show persistent weather events. Over the eastern North Pacific, while the OBS negative LFAs may persist as long as 40 days versus 20 days for the positive LFAs, the MDL LFAs display an opposite behavior, with negative LFAs persisting for a much shorter time than the positive ones (10 days vs 30 days, Fig. 13).

The principal storm tracks as well as the 250-mb mean zonal winds were also examined to supplement the investigation of the large-amplitude LFAs. Contrasted with the observed, the model's U250s display considerable eastward extension over both the North Pacific and the North Atlantic oceans, and their associated storm tracks show substantial equatorward displacement near the jet exit. These model characteristics are consistent with the model's preference for developing large LFAs farther east and southeast of those observed in the real atmosphere.

Skillful prediction on a timescale of two weeks and beyond cannot be achieved until the model correctly

simulates the location of the low-frequency anomalies. Model deficiencies in the simulation of the magnitude of the large LFAs must also be addressed. Naturally, much more effort is needed in order to gain further insight into the physical processes leading to the deficiencies as well as finding ways to improve the model's performance.

Acknowledgments. The authors would like to thank Drs. S. Saha and Z. Toth for making the 10-yr NMC MRF runs available for our present investigation, and also to Drs. G. White, K. Mo, A. Barnston, and D. Walker for their careful reviews and valuable comments on this article.

REFERENCES

Anderson, J. L., 1993: The climatology of blocking in a numerical forecast model. *J. Climate,* **6,** 1041–1056.

Barnston, A. G., and R. E. Livezey, 1987: Classification, seasonality and persistence of low-frequency atmospheric circulation patterns. *Mon. Wea. Rev.,* **115,** 1083–1126.

——, and H. M. van den Dool, 1993: Toward understanding the causes of low frequency variability: The interannual standard deviation of monthly mean 700 mb height. *J. Climate,* **6,** 2083–2102.

Blackmon, M. L., 1976: A climatological spectral study of the 500 mb geopotential height of the Northern Hemisphere. *J. Atmos. Sci.,* **33,** 1607–1623.

——, J. M. Wallace, N.-C. Lau, and S. L. Mullen, 1977: An observational study of the Northern Hemisphere wintertime circulation. *J. Atmos. Sci.,* **34,** 1040–1053.

Chen, W. Y., and Huug M. van den Dool, 1995: Forecast skill and low frequency variability in NMC DERF90 experiments. *Mon. Wea. Rev.,* **123,** in press.

Dole, R. M., and N. D. Gordon, 1983: Persistent anomalies of the extratropical Northern Hemisphere wintertime circulation: Geographical distribution and regional persistence characteristics. *Mon. Wea. Rev.,* **111,** 1567–1586.

Kalnay, E., M. Kanamitsu, and W. E. Baker, 1990: The NMC global forecast system. *Bull. Amer. Meteor. Soc.,* **71,** 1410–1428.

Kanamitsu, M., 1989: Description of the NMC Global Data Assimilation and Forecast System. *Wea. Forecasting,* **4,** 335–342.

Knox, J. L., and J. E. Hay, 1985: Blocking signatures in the Northern Hemisphere: Frequency distribution and interpretation. *J. Climatol.,* **5,** 1–16.

Nakamura, H., and J. M. Wallace, 1990: Observed changes in the baroclinic wave activity during the life cycles of low-frequency circulation anomalies. *J. Atmos. Sci.,* **47,** 1100–1117.

——, and ——, 1991: Skewness of low-frequency fluctuations in the tropospheric circulation during the Northern Hemisphere winter. *J. Atmos. Sci.,* **48,** 1441–1448.

Sela, J. G., 1980: Spectral modeling at the National Meteorological Center. *Mon. Wea. Rev.,* **108,** 1279–1292.

Tibaldi, S., and F. Molteni, 1990: On the operational predictability of blocking. *Tellus,* **42A,** 343–365.

Tracton, M. S., K. Mo, W. Chen, E. Kalnay, R. Kistler, and G. White, 1989: Dynamical extended range forecasting (DERF) at the National Meteorological Center. *Mon. Wea. Rev.,* **117,** 1604–1635.

Van den Dool, H. M., 1991a: Interannual variability in a 10 year run of the NMC model: Global and hemispheric mean surface temperature, precipitation and precipitable water. *Proc. 16th Climate Diagnostics Workshop,* Lake Arrowhead, CA, 247–255.

——, 1991b: Mirror images of atmospheric flow. *Mon. Wea. Rev.,* **119,** 2095–2106.

——, and S. Saha, 1993: On the seasonal redistribution of mass in a 10-year GCM run. *J. Climate,* **6,** 22–30.

——, S. Saha, and Z. Toth, 1991: The climate in a multi-year NMC model run. *Proc. Fifth Conf. on Climate Variations,* Denver, CO, Amer. Meteor. Soc., 511–514.

Vautard, R., B. Legras, and M. Deque, 1988: On the source of midlatitude low-frequency variability. Part I: A statistical approach to persistence. *J. Atmos. Sci.,* **45,** 2811–2843.

Wallace, J. M., and M. L. Blackmon, 1983: Observation of low-frequency atmospheric variability. *Large-Scale Dynamical Processes in the Atmosphere,* Academic Press, 55–94.

White, G. H., 1980: Skewness, kurtosis and extreme values of Northern Hemisphere geopotential heights. *Mon. Wea. Rev.,* **108,** 1446–1455.

Yang, S., and B. Reinhold, 1991: How does the low-frequency variance vary? *Mon. Wea. Rev.,* **119,** 119–127.